Performance Monitoring of a Secant-Piled Wall Using Distributed Fiber Optic Strain Sensing

Hisham Mohamad, A.M.ASCE[1]; Kenichi Soga, M.ASCE[2]; Adam Pellew[3]; and Peter J. Bennett[4]

Abstract: An optical fiber strain-sensing technique, on the basis of Brillouin optical time domain reflectometry (BOTDR), was used to monitor the performance of a secant pile wall subjected to multiple props during construction of an adjacent basement in London. Details of the installation of sensors and data processing are described. Distributed strain profiles were obtained by deriving strain measurements from optical fibers installed on opposite sides of the pile to allow monitoring of both axial and lateral movements along the pile. Methods for analyzing the thermal strain and temperature compensation are also presented. Measurements obtained from the BOTDR were found to be in good agreement with inclinometer data from the adjacent piles. The relative merits of the two different techniques are discussed. **DOI: 10.1061/(ASCE)GT.1943-5606.0000543.**

CE Database subject headings: Monitoring; Retaining structures; Excavation; Piles; Struts; Deformation; Fiber optics.

Author keywords: Monitoring; Retaining wall; Excavation; BOTDR; Sensors; Inclinometer; Piles; Struts; Deformation.

Introduction

Over the last decade, there has been rapid development in the area of smart sensor technologies, in particular by using structurally integrated optical fiber sensors to form the basis for smart structure technology. A variety of sensor configurations have been developed for measurement of strains and deformations in structures [e.g., localized type such as fiber Bragg gratings (Sirkis 1998) and multiplexed long gauge interferometric sensors (Ansari 2005)], whereas examples of distributed sensing schemes are stimulated Brillouin scattering or Brillouin optical time domain analysis (BOTDA) (Bao et al. 2001; Niklès et al. 1996) and Brillouin optical time domain reflectometry (BOTDR) (Mohamad et al. 2010).

In this study, we used a BOTDR sensing system, a distributed strain measurement system that uses a standard single-mode optical fiber and is the basis of the reflective technique. When an optical pulse is launched from the BOTDR analyzer to one end of an optical circuit, it travels along the fiber and a small fraction of the light is backscattered. One of the components of this backscattered light is the Brillouin scattered light. Because the frequency of Brillouin scattering is linearly proportional to the applied strain (Horiguchi et al. 1995), it is possible to obtain the strain distribution from the scattering locations by resolving the back-scattered signal for both frequency and return time of the signal.

Depending on how the measurement of the BOTDR analyzer was set, the system used in this study can measure strain with an accuracy of up to ±30 microstrain along the full length (up to 10 km) of a suitably installed optical fiber. BOTDR can be used with standard inexpensive telecommunication optical fiber cables wrapped around or embedded in structures, in which a single optical fiber potentially replaces a very large number of closely spaced point sensors. Hence, it provides an economic and effective solution and has considerable potential as a system for performance monitoring.

This study presents the novel application of BOTDR strain sensing during the construction of a secant piled wall. The aim of the paper is to demonstrate the suitability of distributed strain measurement in detecting the full mode of deformation of the retaining wall from the measured strain data. The measurement results are validated with inclinometer readings and design analysis.

Field Measurement Site

The site was located on the former BT Telephone Exchange (built between 1955 and 1960) at 21 Chesham Place, Belgravia, London, which was replaced by six substantial single-floor apartments (built between 2005 and 2007) including an underground parking lot. The perimeter bored piles (shown in Fig. S1) were constructed by using minipile technology consisting of temporary casings of 508-mm outer diameter pushed into the clay to the toe of the male/female piles. The male piles that provide the reinforcement were bored with a 475-mm auger and spaced at 600-mm intervals. The secant female piles provided a temporary groundwater cutoff. The wall was supported by three levels of temporary struts when the excavation reached formation level. A base slab was constructed as the fourth level of lateral support. Out of 192 male piles constructed across the perimeter of the wall, eight of them were equipped with inclinometer tubes, whereas optical fiber strain sensors were installed in two piles.

The ground conditions of the site consisted of sand and gravels overlying London clay (as shown later in Fig. S6). The upper sandy gravel was found to be clayey and may be associated with alluvium, whereas the terrace gravels below were classified as

[1]Senior Lecturer, Faculty of Civil Engineering, Univ. Teknologi Malaysia, 81310-UTM Skudai, Johor, Malaysia (corresponding author). E-mail: mhisham@utm.my

[2]Professor of Civil Engineering, Univ. of Cambridge, Dept. of Engineering, Trumpington Street, Cambridge CB2 1PZ, UK. E-mail: ks207@cam.ac.uk

[3]Director, RKD Consultant Ltd, Wigham House, 16-30 Wakering Rd., Barking IG11 8QN, UK. E-mail: adam@rk-d.co.uk

[4]Formerly Univ. of Cambridge. E-mail: pjb65@cam.ac.uk

Note. This manuscript was submitted on May 25, 2010; approved on March 16, 2011; published online on March 17, 2011. Discussion period open until May 1, 2012; separate discussions must be submitted for individual papers. This paper is part of the ***Journal of Geotechnical and Geoenvironmental Engineering***, Vol. 137, No. 12, December 1, 2011. ©ASCE, ISSN 1090-0241/2011/12-1236–1243/$25.00.

medium dense sandy gravel. The London clay appeared to be stiff to very stiff clay with claystones encountered at variable depths. Groundwater was encountered during drilling in the gravels; readings from two standpipes showed that water levels were approximately +2.0 m ordnance datum (OD).

Installation

The fiber optic sensing cable used in this study was a reinforced-ribbon cable manufactured by Fujikura Ltd. [see Fig. 1(a)]. The cable consists of four optical fibers that are reinforced with a pair of steel wires. Only one fiber is required for connection to the strain analyzer, the others provide redundancy. This cable was chosen because of its capability of withstanding the harsh installation conditions, but is still sensitive to strain. Laboratory tests on fiber optic performance embedded in concrete columns have been conducted to validate its performance (Mohamad 2008).

A single optical cable was attached along the two opposing sides of the reinforcement cage by first fixing the cable with two clips at the bottom of the cage [as shown in Fig. 2(a)]. The cable was extended along each side of the cage as it was lowered into the borehole. Once the top section of the cage was positioned just above ground level, the two sections of the cable were pretensioned to approximately 2,000 microstrain and clamped onto the adjacent bars. The prestraining allowed the positions of sensing sections to be identified when reading from the data trace (as shown later in Fig. 4).

To ensure that the optical fibers survived the construction process, a steel pipe installed at the top of pile cage was used to protect the fibers, as shown in Fig. 2(a). This is particularly important while breaking the concrete at the top of the pile during ground excavation. The two ends of the sensing cable were safely stored in a box in which they could later be accessed from the top of the protruding steel pipe and connected to the BOTDR strain analyzer.

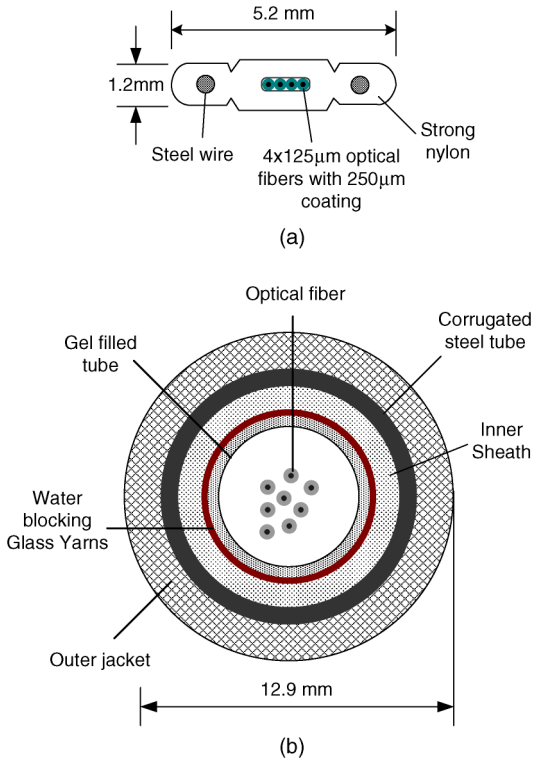

Fig. 1. Fiber optic cables: (a) Fujikura reinforced-ribbon fiber; (b) Unitube cable

In addition to the reinforced-ribbon cable, a standard telecom cable consisting of thick plastic coatings reinforced with steel, around a gel-filled tube containing the optical fibers [Fig. 1(b)] was laid in the pile to act as a temperature-sensing cable. This Unitube cable is insensitive to any mechanical strain because the optical fibers are free to move inside rather than carry strain. However, the cable is still susceptible to thermal effects and hence the temperature profile along the fiber can be obtained.

Fig. 2(b) shows the layout of optical fiber sensors installed at Pile 126 and the inclinometer at Pile 125. Another set of BOTDR and inclinometer measurements were made at Piles 117 and 116. These piles were located at the south of the perimeter wall (supporting foundation pressures of 25 Chesham Place) as shown in more detail in Figs. S1 and S2.

Bending Strain and Axial Strain

By measuring the strain along two fibers placed symmetrically with respect to the axis, it is possible to monitor the full behavior of a diaphragm wall. The plane deformation problem of a pile, with two fibers a and b, is shown in Fig. 3. The measured strains ε_a and ε_b can be used to derive the quantities of lateral component from

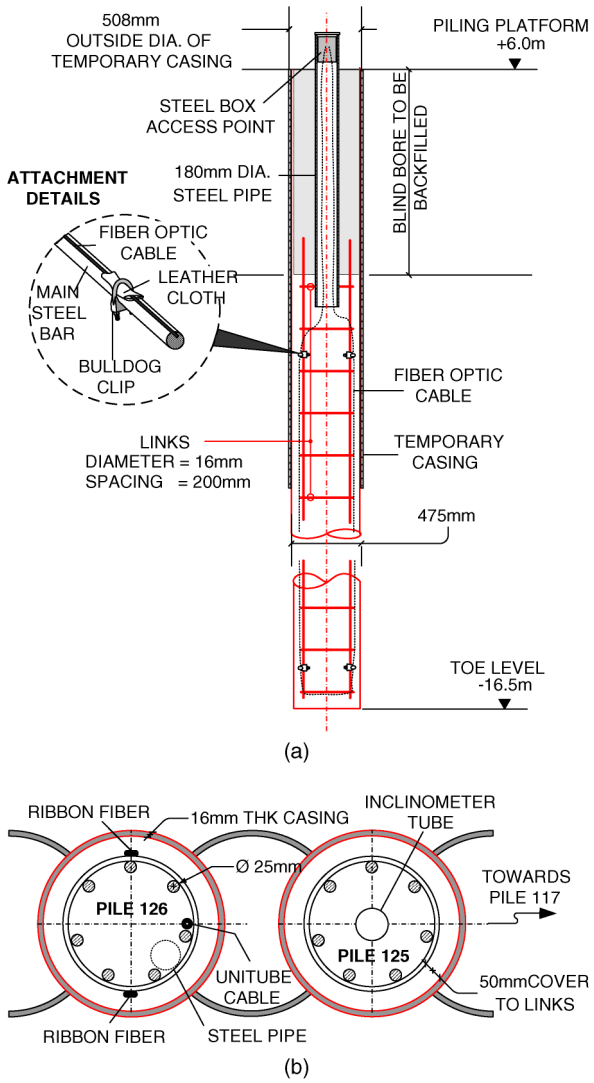

Fig. 2. Layout of fiber optic cables: (a) structural pile layout and fiber optic instrumentation; (b) position of inclinometer and fiber optics

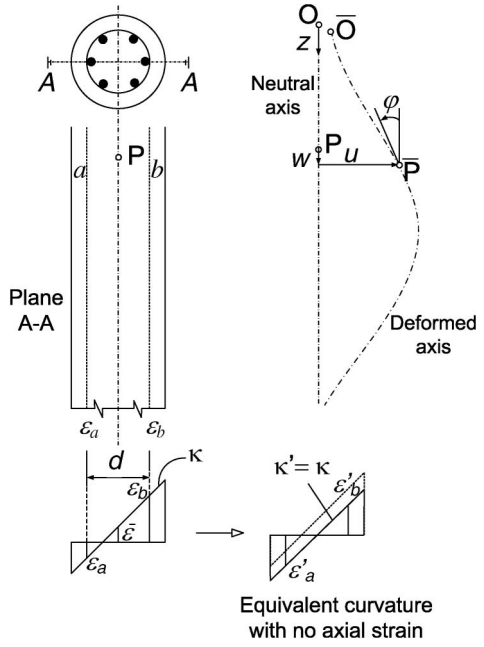

Fig. 3. Determination of plane deformation by measuring strains ε_a and ε_b along fibers a and b

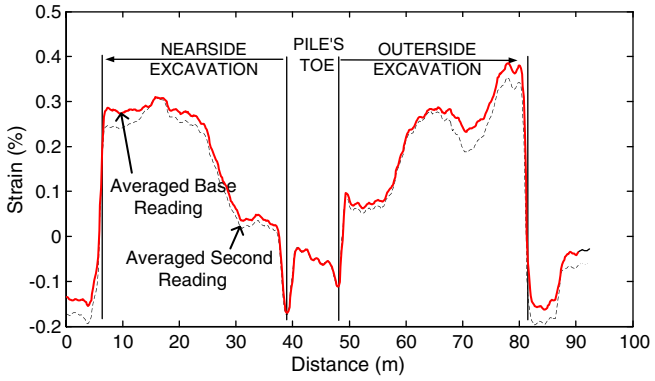

Fig. 4. Actual strains measured in Pile 126; the prestrain/sensing sections are marked as "nearside excavation" and "outerside excavation"

Eq. (1), i.e., the curvature κ, the gradient φ, and the lateral displacement u. The quantities for the vertical component, averaged axial strain $\bar{\varepsilon}$, and vertical displacement w can be obtained from Eq. (2).

$$\kappa = \frac{1}{d}(\varepsilon_a - \varepsilon_b) \qquad \varphi = \int \kappa dz + A \qquad u = \int \varphi dz + B \quad (1)$$

$$\bar{\varepsilon} = \frac{1}{2}(\varepsilon_a + \varepsilon_b) \qquad w = \int \bar{\varepsilon} dz + C \quad (2)$$

The constants A, B, and C can be found by taking further measurements, such as measuring the pile tip displacements by using a total station, or by considering known or assumed boundary conditions.

Temperature Compensation

An example of the actual BOTDR strain measurements of the optical fibers attached along the reinforcing cage is shown in Fig. 4. Tensile strain is assumed as positive. The figure consists of a baseline reading measured before the excavation and a subsequent reading made after the excavation, with each measurement measured three times and averaged to improve the accuracy. The baseline reading shows the prestrain profile applied during the installation. The prestrain was not constant along the pile; the tensile strain was highest at the top but significantly smaller at the bottom. This was most likely because of interactions among the cables and concrete weight in which compressive forces were greater at the bottom of the pile. Hence, the applied tensile force in the cables was reduced near the bottom of the pile. It was also possible that the concrete curing process may have contributed to the uneven strain profile. However, the actual strain regime was not a concern because only the relative strains among a baseline reading and the subsequent readings were considered.

It is known that the Brillouin frequency shift in optical fiber is linearly proportional to strain and temperature. By considering a small unstrained section that ran across the bottommost link, the section in the trace could be used as a quick reference point to compensate for the temperature effect near the pile tip because this section reads thermal strain only. A temperature compensated subsequent reading is shown in Fig. 4. It can be seen that the strain at the pile's tip is exactly similar to the one from baseline reading. The strains measured along the two opposite sides of the pile, on the other hand, changed because the pile was deflected. This method used to compensate for temperature by referring strain at the loose or coiled sections as previously been reported by Bennett et al. (2006) and Ohno et al. (2002).

Fig. 5 shows the axial strains, $\bar{\varepsilon}$ (after applying the temperature compensation at the pile tip), measured in Pile 125 deduced from the BOTDR strain measurements of the two opposite sides of the piles by using Eq. (2). The measurements were made when the excavation depth was at −2.4 m OD (October 11, 2005) and at −4.5 m OD (November 8, 2005) from a baseline reading on August 12, 2005. Pile 117 unfortunately had no measurement measured before the excavation took place, and therefore, comparison can only be made between October 11, 2005, and November 8, 2005 (see Fig. S3).

The averaged axial BOTDR strains indicated that the wall was actually under compression. The compressive strain profile inferred along the neutral axis of the pile could be a combination of (1) mechanical strain from vertical loading; (2) thermal strain generated by temperature variation along the pile's depth; and (3) a temperature compensation component that is inherent to the BOTDR measurement technique. When analyzing the bending behavior of a pile, the variation of thermal strain is usually not a concern because the value will be eliminated after measuring the difference of strains between the two fibers, provided that the temperature between both sides of the wall are equal.

To differentiate different components of BOTDR strain data, the temperature profile along the whole length of the wall is needed, and this can be obtained from a temperature cable installed in the piles. The temperature is calculated by dividing the BOTDR strain with the combined coefficient of thermal expansion of cable, α_{BOTDR} given as

$$\Delta T = \frac{\Delta \varepsilon_T}{\alpha_{\text{BOTDR}}} \quad (3)$$

A detailed account of thermal characteristics of BOTDR and calibration tests on the optical cables used in this study were reported by Mohamad (2008). The coefficient α_{BOTDR} consists of two components, which can be written as

$$\alpha_{\text{BOTDR}} = \alpha_a + \alpha_b \quad (4)$$

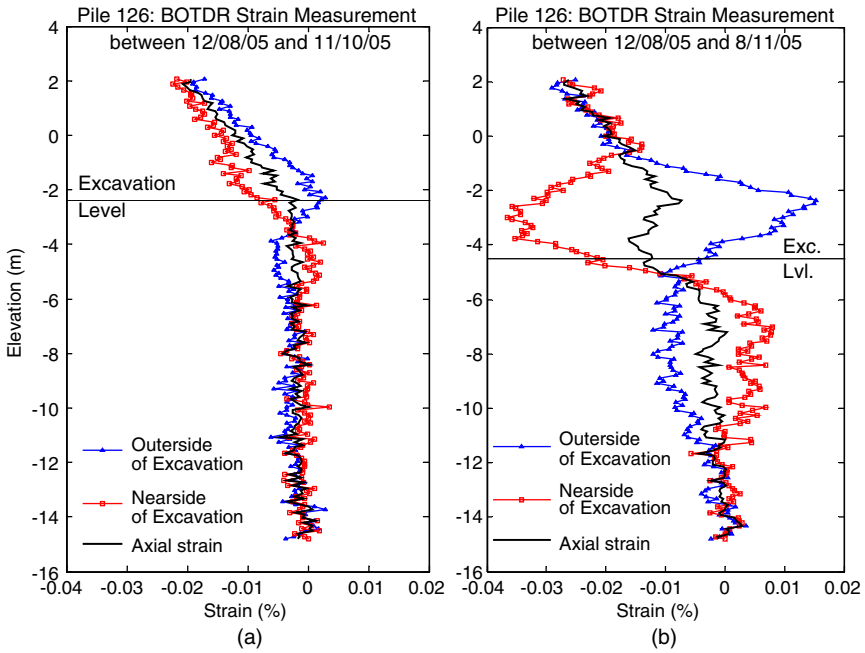

Fig. 5. Bending strains and axial strains in: (a) Pile 126 at −2.4 m OD excavation; (b) Pile 126 at −4.5 m OD excavation

where α_a is the temperature-induced apparent strain of Brillouin frequency shift, and α_b is the thermal expansion coefficient of jacketed fiber.

The first term on the right-hand side of Eq. (4) is a fixed value for all types of optical cables, i.e., $\alpha_a = 19.47 \times 10^{-6}/°C$. This component needs to be removed from the data first. The second term, α_b, depends on the type of jacket and the method of cable installation. For example, the cable thermal expansion, α_b, for reinforced-ribbon and Unitube cable is $23.2 \times 10^{-6}/°C$ and $4.2 \times 10^{-6}/°C$, respectively. However, the value of α_b for reinforced-ribbon cable changes when it is embedded in concrete because the thermal behavior is mainly governed by the concrete thermal expansion coefficient. It is measured as $10 \times 10^{-6}/°C$. The thermal behavior of Unitube cable, on the other hand, is not affected by the installation process because of the presence of a gel layer in the cable tube, which does not allow strain from the buffer to be transferred to the fiber core.

Fig. 6(a) shows an example of temperature changes measured by the temperature cable between August 12, 2005, and November 8, 2005. The temperature difference is obtained by dividing the

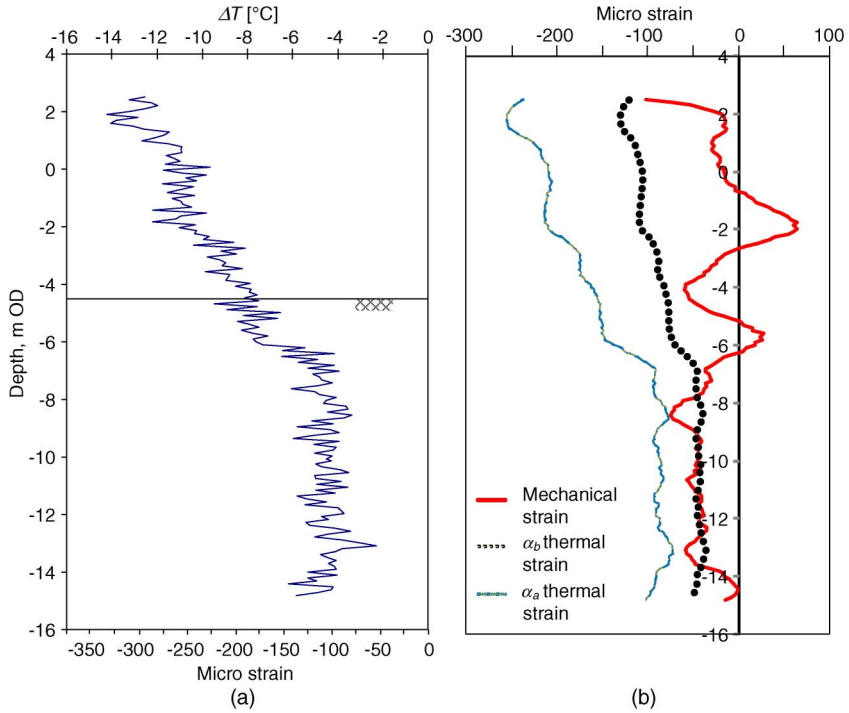

Fig. 6. Thermal strain variation measured in Pile 126 at −4.5 m OD excavation: (a) strain measured in temperature cable; (b) corrected axial mechanical strain

measured BOTDR strain from the temperature cable by $\alpha_{BOTDR} = 23.67 \times 10^{-6}/°C$ [Eq. (3)]. Between the two measurement dates (from summer to fall), it is shown that temperature of the pile had dropped by 5°C inside the ground, whereas temperature reduction was more above the ground and gradually increased toward the pile tip.

In Fig. 6(b), three sets of data are shown: (1) the corrected axial mechanical strain; (2) BOTDR apparent thermal strain; and (3) concrete thermal strain. The concrete thermal strain is calculated by multiplying the temperature [Fig. 6(a)] by $\alpha_b \approx 10\ \mu°C^{-1}$ of the concrete, whereas the apparent thermal strain component is calculated by multiplying the measured temperature changes by $\alpha_a = 19.47 \times 10^{-6}/°C$. To obtain the corrected axial mechanical strain of the wall (that is, strain solely owing to axial force), the two combined thermal strain components were subtracted from the original mean axial BOTDR strain [similar to the one shown in Fig. 5(a), but without temperature compensation at the pile's tip]. As shown in Fig. 6(b), the measurement shows that Pile 126 only experienced a slight mechanical compression of 50 $\mu\varepsilon$, primarily below the excavation level. Thus, the compressive strains previously shown in Fig. 5 are primarily attributed to thermal contraction of the pile, especially toward the top of the pile.

Comparison with Inclinometer Readings

The difference in the strains measured in the fibers on opposite sides of the pile, shown in Fig. 5, can be converted into curvature by using Eq. (1). By integrating the curvature once, the inclination of the pile can be calculated; and by integrating it twice, the lateral displacement of the pile is obtained. For simplicity, the instrumented piles were assumed not to move at the toe and therefore constants A and B (for displacement and rotation) were set as zero. For data comparison, the inclinometer data obtained from the adjacent piles can be differentiated once to get the curvature and integrated once for lateral displacement. In this study, integration on the actual data was done using the trapezoidal rule, whereas the differential method is based on centered differences.

To obtain a realistic comparison of the two measuring systems, inclinometer readings were interpolated or averaged between the two dates, closest to the date of the BOTDR readings. Fig. 7 shows the comparisons of BOTDR and inclinometer readings from Piles 126 and 125 in displacement, gradient, and curvature at the excavation depths of −4.5 m OD. The earlier readings at −2.4 m OD are shown in Fig. S4. In the case of Pile 116, the baseline for the inclinometer readings also had to be adjusted before comparison of strain measurement in Pile 117. The baseline was obtained by averaging readings from October 6, 2005, and October 14, 2005, and this was compared with an average of readings on November 3, 2005, and November 21, 2005, as illustrated in Fig. S5. The lateral displacements, slopes, and curvatures from the two different sets of instrumentation are shown in Fig. 8.

Results from Figs. S4, 7 and 8 indicate that the measurements of the basement wall deformation are similar for BOTDR and inclinometer deflection, gradient, and curvature. The assumptions that there are no displacement and rotation at the pile's toe seem to match both data sets very well. The maximum displacements were found to be approximately 1–1.5 m above the excavated ground level whereas the overall movements recorded throughout the whole stage of construction fall within the acceptable design range.

Analysis versus Measurement

Field measurements were compared with the predicted deformations of the secant wall with the flexible retaining wall analysis program or FREW (www.oasys-software.com/frew/). The two-dimensional (2D), plain strain program incorporates the finite stiffness of the wall with linear elastic-plastic behavior of the ground. Actual ratios of horizontal corner distance to maximum excavation depths for the measured piles are 1 and 1.5, so noticeable three-dimensional (3D) effects were expected. These 3D effects lead to reduced actual (measured) displacements and stresses in the walls. Thus, the analysis is intrinsically conservative. Ground and wall properties used in the analysis were on the basis of the design calculation report (ArupGeotechnics 2005) and are summarized in Fig. S6.

Calculated displacements from the BOTDR measurements were smaller than the FREW calculated values, especially in the early stages of excavation, as shown in Fig. 9. At −2.4 m OD,

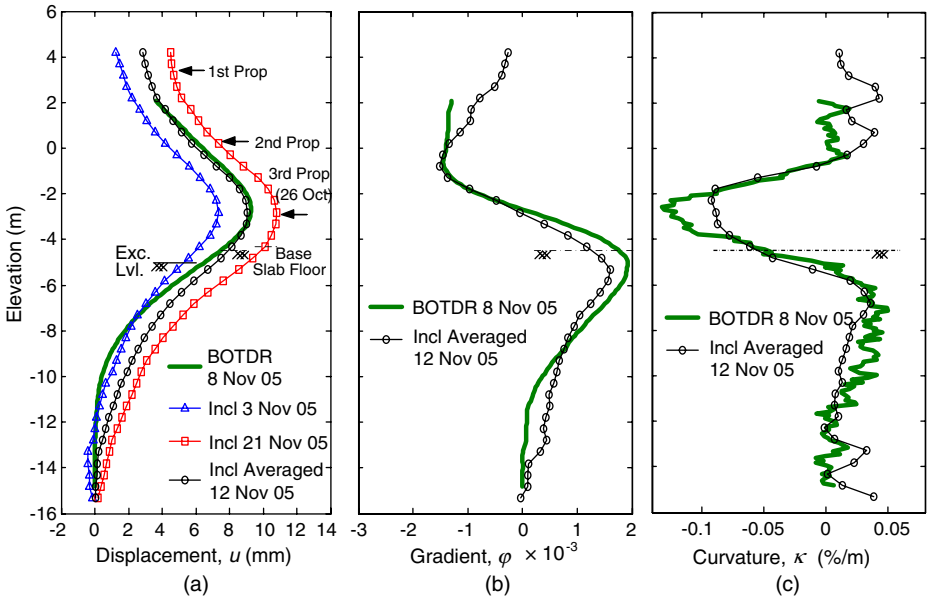

Fig. 7. Comparisons of second strain measurement recorded at Pile 126 and averaged inclinometer readings at Pile 125

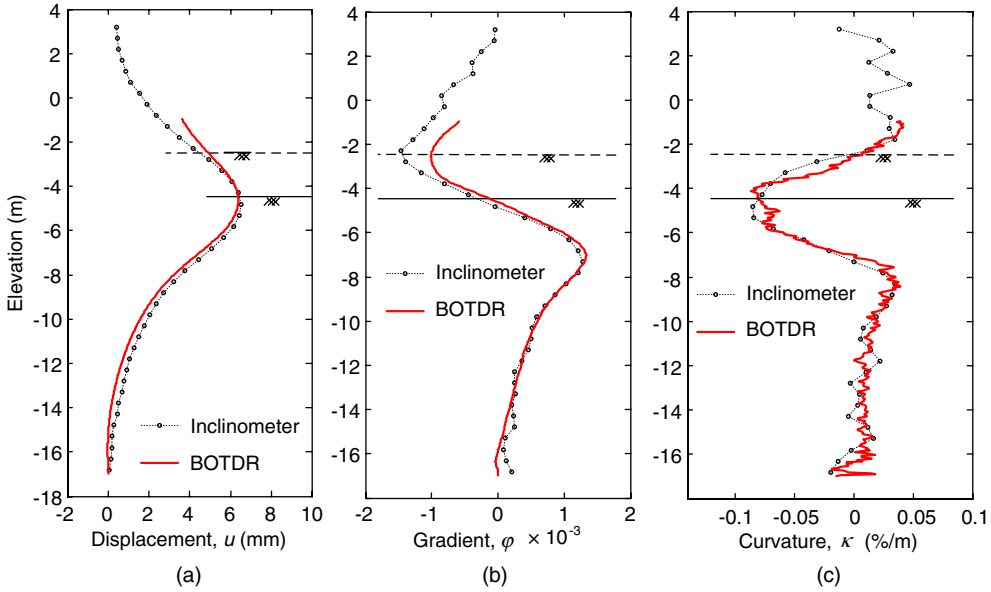

Fig. 8. Incremental movement recorded at Pile 117 (BOTDR) and Pile 116 (inclinometer) between two-staged excavation levels: (a) lateral deflection; (b) inclination; and (c) curvature

the program predicted a maximum lateral displacement of 8.3 mm, compared with 3.0 mm of BOTDR measurement. At −4.5 m OD, FREW deflection calculations yielded 11.8 mm, i.e., 2.5 mm more than the fiber optic measurement. The following reasons for these differences are offered:

1. The building behind the piled wall had both footings and a basement slab that would have acted to restrain horizontal ground movements. The differences would be most apparent in the early stages of excavation when compared with the FREW analysis that ignored this effect.
2. At the time of wall installation, there was more vertical load behind the wall than in front of it. The FREW analysis inaccurately included some horizontal wall movement because horizontal equilibrium was established prior to modeling the subsequent excavation.

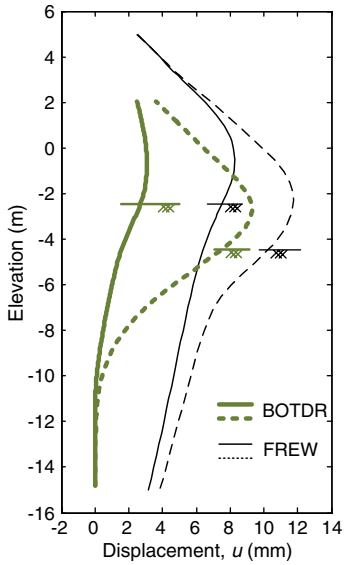

Fig. 9. Comparison of deflection analyses between BOTDR and FREW at −2.4 m and −4.5 m OD at Pile 126

3. In the FREW, the bottom boundary at −20 m OD is fixed but the pile toe is free to move and is seen to displace horizontally in contrast to the measurement method assumption.
4. The FREW does not incorporate a small-strain stiffness soil model, which necessarily leads to some further inaccuracy in full soil-structure analyses.

The calculated bending moment and shear force were much closer to the field data. By using the relationships of $M = -\kappa EI$ and $Q = dM/dz$, the bending moment, M and shear force, Q for Pile 126 are plotted in Fig. 10. In the design calculations, i.e., ultimate limit state (ULS), the wall flexural stiffness (EI) was measured as $0.7E_oI$ during construction and the short-term Young's modulus of concrete, E_o was chosen as 28 GPa as according to CIRIA C580 Report (Gaba et al. 2003). The bending moment profiles [Figs. 10(a) and 10(c)] from BOTDR, inclinometer, and FREW generally agree well. At −2.4 m OD [Fig. 10(a)], the estimation of the maximum bending moment of 50 kNm from FREW was slightly more than the two field measurements of 30 kNm. At −4.5 m OD [Fig. 10(c)], BOTDR displayed the highest bending moment of 125 kNm, whereas the FREW analysis showed a maximum bending moment of 77 kNm, and the inclinometer gave a value between the two (87 kNm).

Because the BOTDR analyzer used in this study produces a random error of ±30 $\mu\varepsilon$, and the measurement is densely plotted at every 10 cm, it is sensible to smooth the data to get an appropriate shear force diagram when differentiating the bending moment. The data points were fitted with a polynomial curve (Savitzky and Golay 1964), which is a second degree of Savitzky-Golay smoothing filtering. Figs. 10(b) and 10(d) compare the differentiated shear force diagram from BOTDR and inclinometer readings, together with the FREW analysis results. The maximum shear forces measured by both BOTDR and inclinometers were found to be slightly smaller than the FREW analysis but still gave its zig-zag shape caused by the strut loads. The actual strut loads can be deduced from the difference between the two peaks at each strut point. In Fig. 10(d), the largest strut load estimated from FREW is 200 kN. It is not possible, however, to infer the resulting strut loads from the inclinometer and BOTDR shear force diagrams.

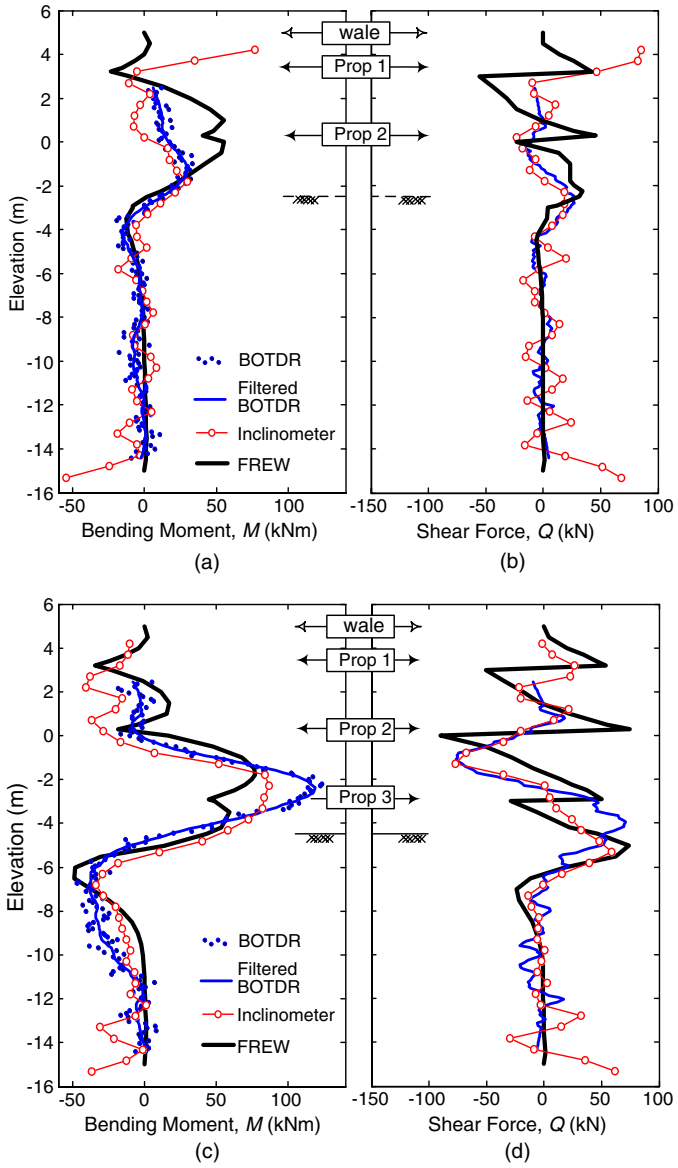

Fig. 10. Bending moment and sheer force diagrams: (a) and (b) at depth of −2.4 m OD; (c) and (d) at depth of −4.5 m OD

The reason that both measurement techniques give less shear force is because that they are unable to detect sharp changes of shear loads. A good shear force measurement would require the instruments make measurements at considerably smaller distance intervals to detect such local events and make precise measurements. In the case of the inclinometer, the spatial resolution is only every half a meter. In the case of the BOTDR, readings can be measured every 5 cm, but the analyzer actually measures a weighted average of strain along approximately 1-m gauge length (Klar et al. 2006).

BOTDR versus Inclinometer

Although the inclinometer and BOTDR measurements are similar, a few important differences resulted in the study. The double-fiber BOTDR geometry yields a direct curvature/bending moment distribution, whereas it is necessary to differentiate the gradient from the inclinometer data. Deriving the shear force diagram, inclinometer data may likely to show less stable results compared with the filtered BOTDR data, especially in measuring small movements such as those presented in Fig. 10(b). The noise of inclinometer data is very large, particularly at the bottom and top of the pile. For example, shear force is usually minimal at the pile tip, but the random error from differentiating inclinometer data twice resulted in shear force of 60 kN at the pile tip.

The other benefit of using BOTDR to measure wall deflection is that the wall can still be monitored long after the construction of basement and ground floors is complete because the optical fiber cables can be buried or carried in ducts and accessed from different locations. Furthermore, the axial behavior of the wall can also be observed, which is not possible when an inclinometer is used. The added advantage of measuring axial deformation indicates that the sensor is able to monitor the three-dimensional deformation both during excavation and later in construction as the superstructure rises and starts to load the wall piles.

The disadvantage of using BOTDR strain sensing is that the derivation of lateral displacement involves acquiring two boundary conditions, i.e., the constants A and B. The inclinometer only requires the knowledge of constant B. This measurement technique requires that the strain profile must be obtained in both optical fibers.

In cost analysis, the cost of the analyzer at present is quite substantial: US$70–150 thousand. However, the cost of a standard optical fiber is very low (from $0.2/m) compared with other point measurement sensors. The BOTDR system may become cost-effective if the analyzer is connected to a large number of fibers or be shared at different sites (Tester et al. 2006).

Conclusion

Measurement of axial and lateral deformation of laterally loaded secant piles was demonstrated by using distributed optical fiber strain sensors based on BOTDR. Axial strain profiles were derived by averaging strain distributions from two optical fiber cables installed on opposing sides of the piles, whereas bending strain profiles were deduced by measuring the difference of the two strains. This paper presents the details of data processing and temperature compensation of Brillouin scattering necessary to calculate strains and ultimately deformation. The results obtained from the strain measurements agreed with that from inclinometer data obtained from adjacent piles. Further calculation of bending moment and shear force showed that BOTDR measurement also agreed with that derived from inclinometer measurement and FREW results. The benefits and the limitations of using distributed optical fiber sensing, as opposed to inclinometers, in retaining walls were discussed. Because of the simple and quick installation technique, distributed optical fiber sensing in piles can be as practical as inclinometer measurements. Further development of optical fiber technology is likely to increase its accuracy and decrease its cost.

Acknowledgments

The writers would like to thank the assistance provided Dr. Assaf Klar and Dr. Eduard Vorster (former members of Cambridge Geotechnical Research Group) during the fiber optic installation process. The writers would like to acknowledge in particular the support provided by Mr. Jim Mackey of McGee Group Ltd and Arup Geotechnics in supporting this work.

Supplemental Data

Figs. S1, S2, S3, S4, S5, and S6 are available online in the ASCE Library (www.ascelibrary.org).

References

Ansari, F. (2005). "Fiber optic health monitoring of civil structures using long gage and acoustic sensors." *Smart Mater. Struct.*, 14(3), S1–S7.10.1088/0964-1726/14/3/001

ArupGeotechnics Report. (2005). "Project Lateral: Calculation report—Basement wall design." *Final Report*, Feb. 2005. Ove Arup & Partners Ltd., London.

Bao, X., DeMerchant, M., Brown, A., and Bremner, T. (2001). "Tensile and compressive strain measurement in the lab and field with the distributed Brillouin scattering sensor." *J. Lightwave Technol.*, 19(11), 1698–1704.

Bennett, P. J., et al. (2006). "Distributed optical fibre strain sensing in piles." *Reuse of foundations for urban sites: Proc., Int. Conf.*, A. P. Butcher, J. J. M. Powell, and H. D. Skinner, eds., Vol. EP73, 105–114, IHS BRE, Watford, UK.

Gaba, A. R., Simpson, B., Powrie, W., and Beadman, D. R. (2003). *CIRIA Rep. C580: Embedded retaining walls: Guidance for economic design*, CIRIA, London.

Horiguchi, T., Shimizu, K., Kurashima, T., Tateda, M., and Koyamada, Y. (1995). "Development of a distributed sensing technique using Brillouin scattering." *J. Lightwave Technol.*, 13(7), 1296–1302.

Klar, A., et al. (2006). "Distributed strain measurement for pile foundations." *Proc. Inst. Civil Eng. Geotech. Eng.*, 159(GE3), 135–144.

Mohamad, H. (2008). "Distributed optical fibre strain sensing of geotechnical structures." Ph.D. thesis, University of Cambridge.

Mohamad, H., Bennett, P. J., Soga, K., Mair, R. J., and Bowers, K. (2010). "Behaviour of an old masonry tunnel due to tunneling-induced ground settlement." *Géotechnique*, 60(12), 927–938.

Niklès, M., Thévenaz, L., and Robert, P. A. (1996). "Simple distributed fiber sensor based on Brillouin gain spectrum analysis." *Opt. Lett.*, 21(10), 758–760.

Ohno, H., Naruse, H., Kurashima, T., Nobiki, A., Uchiyama, Y., and Kusakabe, Y. (2002). "Application of Brillouin scattering-based distributed optical fiber strain sensor to actual concrete piles." *IEICE Trans. Electron.*, E85-C(4), 945–951.

Savitzky, A., and Golay, M. J. E. (1964). "Smoothing and differentiation of data by simplified least squares procedures." *Anal. Chem.*, 36(8), 1627–1639.

Sirkis, J. S. (1998). "Using Bragg grating sensor systems in construction materials and bridges: Perspective and challenges." *Proc., Int. Workshop on Fiber Optic Sensors for Construction Materials and Bridges*, Technomic Publishing Co., Basel, 44–61.

Tester, P. D., Fernie, R., Bennett, P. J., Kister, G., and Gebremichael, Y. (2006). "Brillouin and fibre Bragg grating fibre-optics development at a 'RuFUS' site in London." *Reuse of Foundations for Urban Sites: Proc., Int. Conf.*, A. P., Butcher, J. J. M. Powell, and H. D. Skinner, eds., Vol. EP73, IHS BRE, Watford, UK, 147–158.